

Progressive disgregation of brain networking from normal aging to Alzheimer's Disease.

Independent Component Analysis on FDG-PET data

Marco Pagani^{1,2}, Alessandro Giuliani³, Johanna Öberg⁴, Fabrizio De Carli⁵, Silvia Morbelli⁶, Nicola Girtler^{7,8}, Dario Arnaldi⁷, Jennifer Accardo⁷, Matteo Bauckneht⁶, Francesca Bongioanni⁶, Andrea Chincarini⁹, Gianmario Sambuceti⁶, Cathrine Jonsson⁴, Flavio Nobili⁷

¹*Institute of Cognitive Sciences and Technologies, CNR, Rome Italy*

²*Department of Nuclear Medicine, Karolinska Hospital Stockholm, Sweden*

³*Environment and Health Department. Istituto Superiore di Sanità, Rome, Italy*

⁴*Department of Hospital Physics, Karolinska Hospital, Stockholm, Sweden*

⁵*Institute of Molecular Bioimaging and Physiology - C.N.R. - Genoa Unit. Italy*

⁶*Department of Nuclear Medicine, Department of Health Science (DISSAL), University of Genoa and IRCCS AOU San Martino-IST, Genoa, Italy*

⁷*Clinical Neurology, Department of Neuroscience (DINOEMI), University of Genoa and IRCCS AOU San Martino-IST, Genoa, Italy*

⁸*Clinical Psychology, IRCCS AOU San Martino-IST, Genoa, Italy*

⁹*National Institute of Nuclear Physics (INFN), Genoa section, Italy*

Corresponding author: Marco Pagani, MD, PhD,
Institute of Cognitive Sciences and Technologies, CNR
Via Palestro 32, 00185 Rome, Italy
E-mail: marco.pagani@istc.cnr.it
Tel: +39-06-44362370-5
Fax: +39-06-44595243

Running Title: Brain Networking in Alzheimer's Disease

Word Count: 6260

ABSTRACT

Brain connectivity has been assessed in several neurodegenerative disorders investigating the mutual correlations between pre-determined regions or nodes. The selective breakdown of brain networks during the progression from the normal aging (NA) to Alzheimer's Disease (AD) has also been observed. We implemented Independent Component Analysis (ICA) on ^{18}F -FDG-PET data in five groups of subjects with cognitive state ranging from NA to AD dementia, including mild cognitive impairment patients not converting (ncMCI) and converting (MCI) to mild AD dementia, in order to disclose the spatial distribution of the independent components (ICs) in each cognitive state, and their accuracy in discriminating the groups. We could identify spatially distinct ICs in each group with an increasing generation of new local circuits proportional to the severity of the disease. AD-specific ICs appeared from the late MCI stage and could discriminate MCI and AD dementia from ncMCI with an accuracy of **83.5%**. There was a progressive disgregation of the intrinsic networks from NA to MCI and AD dementia, in an inversely proportional fashion to conversion time.

Functional brain connectivity on FDG-PET has been shown by ICA to be gradually disrupted across progressive states of cognitive severity in AD, which might be implemented at individual level, especially for prognostic purposes, and as a surrogate biomarker in intervention trials.

Keywords: FDG-PET, Independent Component Analysis, normal aging, mild cognitive impairment, Alzheimer's Disease

INTRODUCTION

Neuronal activity involving different brain regions relies on dynamic communication through both short- and long-range networks establishing temporal or spatial connections (1). Connectivity can be investigated by identifying significant signal intensity correlations between *a priori* defined regions (volumes of interest, VOIs), as segmented by brain atlases (2-5), or between regions resulting from statistical preprocessing (e.g. graph analyses in which brain areas are considered as nodes). By applying the latter techniques to datasets including subjects ranging from normal aging (NA) to mild cognitive impairment (MCI) and Alzheimer's Disease (AD) a selective breakdown of intrinsic brain networks during the progression of AD has been revealed (5,6).

Patients presenting with cognitive impairment do not always progress to overt dementia, but sometimes are stable after years of follow-up or even revert to a normal state (7) constituting an ideal control group for studies on decline from 'progressive' MCI to AD dementia.

Most phenomena that occur in the real world are mixtures of different, often relatively independent, processes. Typical examples are the sounds in a room in which several people are talking simultaneously (the paradigmatic cocktail party model, (8)). Analogously, a distribution of signal intensities across the brain will be a mixture of the activations of a large number of independent neural networks. Under certain conditions, these elementary signals can be recovered by Independent Component Analysis (ICA), a data driven technique that blindly separates mixed signals into independent sources without requiring any *a priori* topographic assumption.

Submitting functional Magnetic Resonance Imaging (fMRI) data to ICA helped disclose a strong functional architecture in all stages of aging from normal status to AD (9). The take-over of local systems on long-distance brain connections speaks in favour of a functional segregation of

neuronal processes. However, it is still not known if there is a *continuum* in the intrinsic network modification associated with AD. In a previous study (10) we reported a continuous loss of order along the disease severity axis in the metabolic set-up of the brain, as assessed using ^{18}F -2-fluoro-2-deoxy-D-glucose positron emission tomography (FDG-PET) and applying a coarse grain thermodynamic approach. Here we examine a possible association between those findings and intrinsic network changes by analyzing the connectivity dynamics.

The aim of the present study was to use FDG-PET to evaluate (i) the spatial distribution of the ICs in subjects ranging from NA to AD dementia, including ncMCI and mild cognitive impairment patients converting (MCI) to mild AD dementia and (ii) the accuracy of the ICs in discriminating between such five groups of subjects with different conditions. Our hypothesis was that the progressive derangement of brain connectivity during the course of the disease is already detectable at the MCI stage and that metabolic patterns identified in MCI patients can help in predictions about the speed of conversion to AD-dementia.

MATERIALS AND METHODS

Participants

Forty two normal elderly subjects (NA), twenty seven nMCI patients, thirty seven MCI patients that converted to AD dementia after more than 2 years since the PET scan (eMCI), fifty eight MCI patients that converted to AD dementia within 2 years since the PET scan (IMCI) and fifty four patients with mild AD dementia at the time of PET scan (AD) were included in the study (Table 1). Exclusion criteria for the same groups of patients were previously described (10). The study was

approved by the institutional review board and all subjects gave their consent to undergo FDG-PET in the framework of a long-term observational study.

MCI patients

MCI patients were subjects referred to our memory clinic for a first diagnostic assessment of a memory complaint. They underwent a complete clinical and neuropsychological diagnostic work-up according to current standards. The baseline evaluation included blood and urine tests, morphological (MRI) and functional (FDG-PET) neuroimaging. They all underwent extensive neuropsychological testing, investigating: (i) categorical and phonological verbal fluency; (ii) executive functions; (iii) visuospatial abilities; (iv) attention and working memory.

Patients were included in the MCI group if they showed impairment in a memory test, either with (multi-domain amnesic MCI) or without (single-domain amnesic MCI) involvement of other cognitive domains, but were not demented. We included only patients that were followed up by regular control visits over at least five years or until they developed AD dementia.

AD dementia patients

The AD dementia patients were subjected to the same tests as for MCI patients and were those diagnosed with mild AD dementia at their first work up at our memory clinic. The presence of dementia was established by clinical interviews with the patient and caregivers, by activities of daily living and instrumental activities of daily living questionnaires, and by the Clinical Dementia Rating scale. The Mini-Mental State Examination (MMSE) was used to score global cognition. Only patients with MMSE score ≥ 19 (mild dementia) attributed to AD according to the NIAAA criteria were

included in the study.

Controls

The control subjects were carefully checked by clinical examinations and the same exclusion criteria used for the patients were used, with the exception of cognitive complaints. Similarly, only subjects with a normal MMSE score (i.e. >26) and with a Clinical Dementia Rating of 0 were considered. They underwent both FDG-PET and MRI and were administered the same extended neuropsychological testing (11).

18F-FDG PET Protocol and Preprocessing.

FDG-PET images were submitted to the preprocessing steps in the Statistical Parametric Mapping (SPM8) stand-alone version (Wellcome Department of Cognitive Neurology, London, UK). Spatial normalization was performed by a customized brain FDG-PET optimized for dementia patients (12) and images were then smoothed with a 8-mm isotropic Gaussian filter to blur individual variations in gyral anatomy and to increase the signal-to-noise ratio.

Statistical Analysis

Among the administered neuropsychological tests we compared in the three MCI subgroups by one-way analysis of variance scorings of Mini Mental State Examination, Rey Auditory Verbal Learning Test immediate total recall, Rey Auditory Verbal Learning Test delayed recall, as well as Trail Making Tests Part A and B, assessing verbal memory and executive functions, respectively.

Statistical Parametric Mapping (SPM)

Brain PET from ncMCI were compared on a voxel-by-voxel basis to those from all MCI by the “two-sample t-test” design of SPM8 implemented in Matlab R2014a (MathWorks, Natick, Massachusetts, USA). The threshold of significance was set at $p < 0.05$, corrected for multiple comparisons with family wise error (FWE). Age and **gender** were considered as confounding variables.

Independent Component Analysis

ICA is based on the assumption that the observed variables in a mixture (the distribution of voxels intensities in PET investigations) are generated by different, mutually independent, underlying ‘sources’. Thus, the deconvolution (de-mixing) of the observed signal as an explicit summation of independent components reveals the ‘hidden structure’ of the observed phenomenon. ICA can be applied in the spatial dimension, as in our case, where the extracted independent components point out highly connected networks.

Spatial ICA of the preprocessed FDG-PET images was performed using the GIFT toolbox (<http://mialab.mrn.org/software/>) as previously described (13). In brief data from each subject were submitted to principal component analysis (PCA) then independent spatial components (ICs) were estimated (8). The number of components was set to 20, intensity values in each voxel was converted to z-scores and images visualized at a thresholded of $z > 3.3$ ($p < 0.001$) creating binary masks. From the resulting components, those with either pathophysiological or anatomo-functional meaning were separately selected in each group and each component was named according to its anatomy, allowing for separate solutions. The remaining ICs were discarded as statistical noise. The number and the extension in voxels of the ICs were correlated to the variance explained by the first principal component of each group (10).

Principal Component Analysis (PCA)

In a previous investigation PCA, separately applied to the same experimental groups, highlighted the presence of a first principal component (PC1) explaining by far the greater part of the system variance (10) and being regarded as the amount of ‘global order’ of brain metabolism. Here we build upon the complementarity of ICA and PCA, with the former having a mainly local character (focus on the enucleation of independent circuits) and the latter a global spectral character.

Support Vector Machine Analysis (SVM)

The IC masks of the AD dementia group, considered to be the most appropriate reference for the aim of the study, were segmented and applied to each of the 218 subjects to compare the intensity values between groups. The FDG uptake in each of the VOIs pinpointed by IC masks was assessed in all five groups implementing an in-house created Matlab-based script that automatically processed mean FDG uptake signal intensities (14). Mean uptake values for the VOIs associated with the selected ICs in NA were analyzed by repeated-measures regression in order to correct values in each subject for the effect of age and gender. Corrected values were then submitted to Support Vector Machine (SVM) discriminating: 1) NA *versus* all patients with AD pathology, thus also including eMCI and lMCI; 2) ncMCI *versus* all patients with AD pathology; 3) ncMCI *versus* NA. In comparisons 1 and 2 we considered both eMCI and lMCI as affected by AD pathology, in line with the concept of presence of AD pathology in the pre-dementia stages (15). Stepwise selection procedure was applied to search for the best sets of components in a SVM model. The performance of each model was evaluated by computing the Receiver-Operating-Characteristic (ROC) curve with relevant area under the curve

(AUC) and sensitivity, specificity and accuracy associated to the best point on the curve with their confidence intervals (C.I.). All these parameters were evaluated following “leave-one-out” cross-validation and each subject was classified by a model fitted to all remaining ones. Each model was also applied to the group/s excluded from the training set. For example, the first model, based on the contrast between NA and all AD, was then applied to ncMCI. SVM, applied by radial basis function kernel, and following ROC curve analysis and accuracy measurements were performed by using the Statistics Toolbox of Matlab R2015b (MathWorks, Natick, Massachusetts, USA).

RESULTS

Demographic data are reported in Table 1.

Mini Mental State Examination ($p < 0.05$), Rey Auditory Verbal Learning Test immediate total recall ($p < 0.005$) and Rey Auditory Verbal Learning Test delayed recall ($p < 0.001$) showed significant changes among the three MCI groups with a progressive decline from ncMCI to lMCI. On the other hand, no significant changes were found for both Trail Making Tests Part A and B, although there was a trend to higher (worse) scores for eMCI and lMCI.

Statistical Parametric Mapping

SPM analyses confirmed in all comparisons the well-known differences between NA and MCI or AD dementia (results not shown). When ncMCI were compared to MCI converting to AD dementia (eMCI + lMCI) highly significant hypometabolism ($FWE_{corrected} p < 0.001$ at both voxel and cluster level) was found in the latter group in bilateral temporoparietal and posterior cingulate cortices (**Fig. 1**)

ICA

Since none of the negative ICs had any pathophysiological significance we selected and discussed only positive ICs, displayed by group in the Supplementary Fig. 1-5.

Table 2 reports the ICs obtained when ICA was applied to the 5 groups of subjects.

Briefly the number of ICs progressively increased from NA to AD dementia patients from six in NA to nine in both ncMCI and eMCI to fourteen in both lMCI and AD dementia patients. Also, the number of voxels composing the ICs progressively increased from NA (17.491) to AD dementia patients (51.740). We highlight here only the ICs with pathophysiological significance, mentioning the brain regions included in them (details in Table 2).

PCA

The decrease in global order (revealed by Lambda1, the first principal component, index of global connectivity) scaled very well with the onset of local neural circuits (revealed by ICs). There was a highly significant inverse correlation between the percent of variance explained by Lambda1 and extension of the ICs in each group ($r=0.975$; $p<0.005$) as well as between Lambda1 and their number ($r=0.961$; $p<0.009$) (Fig. 2A). When these latter were compared with the severity of cognitive impairment, the correlation was positive ($r=0.97$; $p<0.007$) while the mean extension of the ICs in each group showed a constant increase towards AD dementia, with the exception of ncMCI whose ICs were relatively small (Fig. 2B).

Support vector machine

The 14 VOIs drawn from AD-related ICA masks were the input for SVM analysis. SVM highlighted left temporal cortex, as the most accurate ICs in distinguishing NA and ncMCI patients from all AD (Table 3). The discrimination capability reached the highest accuracy with 4 ICs, then

remaining stable or decreasing (due to overfitting). A set of 4 regions, namely bilateral sensorimotor, Precuneus(PC)/ posterior cingulate cortex (PCC) and sylvian temporal cortices, and left temporal cortex (Fig. 3), yielded the highest accuracy both when the comparison was between NA and all AD and between ncMCI and all AD. Table 3 (bottom panel) shows the percent distribution of the subjects in each of the five groups, according to the binary classification of each model. In each SVM model the percentage of subjects classified as AD (thus also including eMCI and lMCI) increased with illness severity. The ROC curves showed high discrimination for NA *versus* all AD and for ncMCI *versus* all-AD (AUC 0.931 and 0.894, respectively) and a rather poor discrimination between ncMCI and NA (AUC .65; Figure 4). However, this model was able to progressively include patients of the other groups into the ncMCI class (non-NA class) proportionally to the increasing illness severity (up to 90% for lMCI and AD dementia patients, data not shown).

DISCUSSION

ICA has identified spatially distinct clusters of voxels with meaningful pathophysiological value in each of the investigated groups. This allowed to uncover the spatial distribution of the ICs in each cognitive status and to assess the accuracy of ICA in discriminating between groups. The hypothesis of a progressive disintegration of brain connectivity during the course of the disease was proven in terms of the generation of new local circuits progressively replacing the ‘brain-as-a-whole’ mean field detected in a previous study (10).

With increasing disease severity, the ‘shared portion’ of brain metabolism (Λ_1) loses in relative importance with respect to local distinct neural circuits, which increase in both number and extension. Basically, functional connectivity degradation in AD progression is a loss of integration: the brain becomes more and more segmented into independent metabolic areas.

The disgregation of the intrinsic networks that characterize NA was progressively more severe moving from ncMCI to AD dementia, with the extension of the ICs being inversely proportional to time distance from conversion. Neurodegenerative processes affect modular networks, rather than isolated regions (16). Long-distance interregional metabolic correlations are impaired by the anatomofunctional progression of neuronal and white matter fibers degeneration (17) causing local compensatory networks to take over, increasing the anatomical and functional segregation of brain processes.

The progressive disintegration of the “giant component” that accounts for the main whole brain connectivity present in NA was disclosed by ICA, which identified in all groups a specific set of FDG-PET-derived components whose pattern was in agreement with the metabolic decay from NA to MCI to AD dementia.

ICs including the primary visual cortex and cerebellum are present in all groups. Therefore, they are not implicated in the functional pattern of cognitive decline. This confirms well-known findings, and supports the suitability of choosing the cerebellum as a normalizing factor in radionuclide functional imaging investigations in AD (18).

The medial frontal gyrus and dorsolateral frontal cortex, DLFC, (representing the anterior portion of the Default Mode Network, DMN) as well as the supplementary motor cortex are incorporated in ICs peculiar to NA. The anterior portion of the DMN is thus disgregated in all patient groups, including ncMCI. The disappearance of anterior DMN in ncMCI is intriguing and may point to the involvement of anterior frontal regions in a variety of conditions, ranging from late-life depression to cerebrovascular disease that affect these networks. However, Di et al (19) reported the absence of the

anterior part of DMN in PET but not in fMRI investigations as being due to their different temporal scales.

On the other hand, posterior cingulate cortex (PCC) and inferior parietal lobule (iPL), among the main components of the posterior portion of the DMN, belong to the same IC in NA and ncMCI. Such IC is disgregated in MCI converters and in AD dementia patients in whom the PCC stands alone in an IC or in association with PC. This is in agreement with the disappearance of DMN in AD and with the knowledge that metabolic changes in the PCC and PC are indeed markers of AD pathology (20).

In line with this interpretation the DLFC, either alone or in association with superior parietal lobule (sPL) or temporal cortex, is embedded in ICs found in all MCI patients, either converting or not. Thus, it may be considered as a correlate of cognitive impairment not specifically linked to AD pathology.

Surprisingly, also the temporal cortex close to the sylvian fissure was embedded in an IC in all patients with cognitive deficit, including ncMCI. Hence it could be considered as a correlate of memory deficit independent of AD pathology, possibly resulting from an aspecific temporal lobe atrophy that is shared by different pathological conditions (21).

The temporal cortex and iPL in the right hemisphere are aggregated in an IC in all groups progressing to AD and in AD dementia itself, and thus are more related to the specific AD signature, independent of the severity of the disease.

Three ICs characterize the late MCI stage, namely those including the lateral occipital cortex bilaterally, the left superior parietal, temporal cortices and PC, and the dorsolateral frontal cortex. The spreading of functional deficit to these association cortices follows the progressive disconnection

hypothesis as proposed by the classical Braak & Braak model (22). Furthermore, PCC (either with or without PC), ventrolateral frontal cortex (VLFC), sPI and medial temporal lobe (MTL), are the ICs specific for the late stage of the disease (lMCI and AD dementia).

The final metabolic signature of the definitive conversion to AD are two ICs including the left temporal cortex. However, the full AD stage includes several ICs: bilateral PC/PCC, MTL, VLFC, iPL, temporal sylvian cortex, and right temporal and occipital lateral cortex.

Beyond the pathophysiological significance of these ICs in AD, two further observations have to be made. First, all three groups of MCI patients were investigated by FDG-PET at a time the neuropsychological assessments showed similar cognitive deficit levels (baseline), with the expected decline from ncMCI to lMCI of memory performances. This makes this study prospective in nature. It shows that the metabolic pattern at baseline was predictive of whether or not the patients would convert to AD dementia and that it was associated to the conversion time. The inclusion of both converting and non-converting MCI patients adds clinical value to the analysis since these intermediate classes are the most relevant targets for a proper and timely diagnosis as well as for subsequent patient management. In the present study, there was a highly significant metabolic difference in the voxel-based analyses in the posterior cingulate and the temporal and parietal cortices between these two groups (Fig. 1). Furthermore, this difference was confirmed by SVM analysis in which analogous regions separated ncMCI and all AD with an accuracy of 83.5% (Table 3).

The IC aggregating PCC and iPL, representing the posterior DMN, is considered to be a “hub” of functional connectivity largely suffering from synaptic disconnection (23) and it was found in a MRI ICA study to best predict the conversion from stable to progressing to AD MCI patients (24).

Second, the FDG-PET uptake in the ICs of AD patients showed a fairly good discriminative power in differentiating NA and ncMCI from the AD groups. This confirms the utility of such data-driven methodology to uncover correlations with pathophysiological meaning (Table 3). Several studies have implemented automated image-based classification methods aimed at differentiating dementia and MCI patients from healthy controls attaining a statistical accuracy of 90% in discriminating AD dementia patients from controls (25-27). When MCI patients that later converted to AD dementia were investigated by unimodal biomarkers the reported discrimination from healthy controls ranged between 80% (28) and 91% (29). In the present study, the ICs derived by the AD dataset showed an accuracy of 90% in discriminating NA and ncMCI from the whole AD pathology cohort. Moreover, the weak discrimination (AUC 0.65) between NA and nMCI indicates a high similarity between these two groups providing functional support for the lack of conversion observed clinically in the latter group.

It is worth noting that when the analyses were modeled on the two extreme classes (NA and AD dementia), the patients of the intermediate groups were progressively assigned to the dementia class according to disease severity and the same held true when the analyses were modeled on ncMCI and AD dementia (Table 3), which confirms the reliability of the present approach.

Our results are consistent with a MRI study performed by Pereira et al. (30) that found in two large multicenter cohorts a progressive decomposition of the connectivity of brain functional networks in groups of patients with the same characteristics as the present investigation, including ncMCI with a follow up of 1 and 3 years. The most striking similarity with our study was the finding of a modularity progressively increasing with the severity of the disease, which suggested a decomposition of whole brain networks into segregated components. This consistency is even more remarkable if we take into

consideration that Pereira et al. adopted a different data analysis strategy (graph analysis) and, more important, a different biological observable (MRI).

Some of the ICs found in the present study were superimposable to those found by Laforce et al (31), one of the very few investigations in which ICA has been implemented in FDG-PET. In that study ICs including the frontotemporal, bilateral occipito-parietal, PCC-PC-Ps cortex and bilateral cerebellum were identified in 46 AD patients. On the other hand, only one study attempting to use ICs to discriminate controls from AD patients recruited within the Alzheimer's Disease Neuroimaging Initiative could discriminate the two groups with an accuracy of 91% (32).

Unlike multicenter studies, the diagnostic procedures in this investigation were very uniform since they were performed by the same clinical group. Additionally, all FDG-PET scans were performed using the same camera minimizing the likelihood that inhomogeneous subject samples and camera acquisitions could have impacted on data variability and results robustness. Another strength of this study is the long follow-up time (minimum 5 years) available for the ncMCI patients, which renders the presence of some late-converter patients unlikely in this group.

The progressive increase of the number of ICs with the disease severity is the functional consequence of the observed loss of relevance of the 'brain-as-a-whole' component we observed in the previous work (10). The degradation of the 'average correlation field' encompassing the entire brain resulted in the creation of local (and largely autonomous) networks. The progressive loss of connectivity of brain metabolism caused by AD can thus be interpreted not as a loss of local correlation inside functional network but by a loss of coordination among networks themselves. Furthermore, in neurodegenerative disorders, ICA-derived patterns can be not only of high diagnostic utility but can also give a mechanistic insight into the etiology of the various diseases (13).

From a methodological point of view, it is worth noting how the present result could be achieved thanks to the complementary properties of PCA and ICA. The emphasis of PCA is on the correlation between the different variables (e.g. brain regions, bins of a spectrum) in time and/or space. A latent physical process is considered to be a global order parameter (in physical terms, a force) imposing a correlation to otherwise independent pieces of information. The contemporaneous presence of independent forces shaping the observed system allows us to consider each variable as a weighted sum of the same hidden order parameters (principal components) acting on the different parts of the system. For ICA the ‘signature’ of an elemental signal is its multimodality. For PCA the ‘strength’ of each elemental signal is the amount of correlation it imposes on the whole system. This difference makes ICA dissect the system into separate local correlation circuits (networks), while PCA tries to recollect the complexity of the system into the minimum number of orthogonal components acting on all the elements (even though with different strengths). This implies that while ICA is, by definition, blind to global average mean field effects (size components) shared by the entire system, PCA is by far less sensitive in catching the presence of local networks. Here we have shown the added value of comparing ICA and PCA pictures to disclose the connectivity dynamics of brain metabolism.

CONCLUSION

FDG-PET is a robust tool for predicting the long-term fate of patients presenting with amnesic MCI at a memory clinic, whether or not they convert to AD dementia in a variable length of time. As such, it is a valuable tool not only for diagnostic purposes but also for prognosis. The ICA and PCA approaches yielded high accurate discriminations among groups, documented the progressive

disgregation of connectivity networks from a healthy brain to AD, and might be proposed as a surrogate biomarker with predictive value for interventional trials.

ACKNOWLEDGEMENTS

The authors wish to thank Professor Stone-Elander for helping in English editing.

REFERENCES

1. Damoiseaux JS, Rombouts SA, Barkhof F, et al. Consistent resting-state networks across healthy subjects. *Proc Natl Acad Sci U S A*. 2006;103:13848-13853.
2. Huang C, Eidelberg D, Habeck C, et al. Imaging markers of mild cognitive impairment: multivariate analysis of CBF SPECT. *Neurobiol Aging*. 2007;28:1062-1069.
3. Nobili F, Salmaso D, Morbelli S, et al. Principal component analysis of FDG PET in amnesic MCI. *Eur J Nucl Med Mol Imaging*. 2008;35:2191-2202.
4. Pagani M, Salmaso D, Rodriguez G, Nardo D, Nobili F. Principal component analysis in mild and moderate Alzheimer's disease--a novel approach to clinical diagnosis. *Psychiatry Res*. 2009;173:8-14.
5. Wang K, Liang M, Wang L, et al. Altered functional connectivity in early Alzheimer's disease: a resting-state fMRI study. *Hum Brain Mapp*. 2007;28:967-978.
6. Hahn K, Myers N, Prigarin S, et al. Selectively and progressively disrupted structural connectivity of functional brain networks in Alzheimer's disease - revealed by a novel framework to analyze edge distributions of networks detecting disruptions with strong statistical evidence. *Neuroimage*. 2013;81:96-109.

7. Pagani M, Dessi B, Morbelli S, et al. MCI patients declining and not-declining at mid-term follow-up: FDG-PET findings. *Curr Alzheimer Res.* 2010;7:287-294.
8. Brown GD, Yamada S, Sejnowski TJ. Independent component analysis at the neural cocktail party. *Trends Neurosci.* 2001;24:54-63.
9. Rombouts SA, Damoiseaux JS, Goekoop R, et al. Model-free group analysis shows altered BOLD FMRI networks in dementia. *Hum Brain Mapp.* 2009;30:256-266.
10. Pagani M, Giuliani A, Oberg J, et al. Predicting the transition from normal aging to Alzheimer's disease: A statistical mechanistic evaluation of FDG-PET data. *Neuroimage.* 2016;141:282-290.
11. Picco A, Polidori MC, Ferrara M, et al. Plasma antioxidants and brain glucose metabolism in elderly subjects with cognitive complaints. *Eur J Nucl Med Mol Imaging.* 2014;41:764-775.
12. Della Rosa PA, Cerami C, Gallivanone F, et al. A standardized [18F]-FDG-PET template for spatial normalization in statistical parametric mapping of dementia. *Neuroinformatics.* 2014;12:575-593.

13. Pagani M, Oberg J, De Carli F, et al. Metabolic spatial connectivity in amyotrophic lateral sclerosis as revealed by independent component analysis. *Hum Brain Mapp.* 2016;37:942-953.
14. Pagani M, Chio A, Valentini MC, et al. Functional pattern of brain FDG-PET in amyotrophic lateral sclerosis. *Neurology.* 2014;83:1067-1074.
15. Sperling RA, Aisen PS, Beckett LA, et al. Toward defining the preclinical stages of Alzheimer's disease: recommendations from the National Institute on Aging-Alzheimer's Association workgroups on diagnostic guidelines for Alzheimer's disease. *Alzheimers Dement.* 2011;7:280-292.
16. Seeley WW, Crawford RK, Zhou J, Miller BL, Greicius MD. Neurodegenerative diseases target large-scale human brain networks. *Neuron.* 2009;62:42-52.
17. Fischer FU, Wolf D, Scheurich A, Fellgiebel A, Alzheimer's Disease Neuroimaging I. Altered whole-brain white matter networks in preclinical Alzheimer's disease. *Neuroimage Clin.* 2015;8:660-666.
18. Soonawala D, Amin T, Ebmeier KP, et al. Statistical parametric mapping of (99m)Tc-HMPAO-SPECT images for the diagnosis of Alzheimer's disease: normalizing to cerebellar tracer uptake. *Neuroimage.* 2002;17:1193-1202.

19. Di X, Biswal BB, Alzheimer's Disease Neuroimaging I. Metabolic brain covariant networks as revealed by FDG-PET with reference to resting-state fMRI networks. *Brain Connect.* 2012;2:275-283.
20. Koch K, Myers NE, Gottler J, et al. Disrupted Intrinsic Networks Link Amyloid-beta Pathology and Impaired Cognition in Prodromal Alzheimer's Disease. *Cereb Cortex.* 2015;25:4678-4688.
21. Mummery CJ, Patterson K, Price CJ, Ashburner J, Frackowiak RS, Hodges JR. A voxel-based morphometry study of semantic dementia: relationship between temporal lobe atrophy and semantic memory. *Ann Neurol.* 2000;47:36-45.
22. Braak H, Braak E. Staging of Alzheimer's disease-related neurofibrillary changes. *Neurobiol Aging.* 1995;16:271-278; discussion 278-284.
23. Drzezga A, Becker JA, Van Dijk KR, et al. Neuronal dysfunction and disconnection of cortical hubs in non-demented subjects with elevated amyloid burden. *Brain.* 2011;134:1635-1646.
24. Willette AA, Calhoun VD, Egan JM, Kapogiannis D. Prognostic classification of mild cognitive impairment and Alzheimer's disease: MRI independent component analysis. *Psychiatry Res.* 2014;224:81-88.

25. Arbizu J, Prieto E, Martinez-Lage P, et al. Automated analysis of FDG PET as a tool for single-subject probabilistic prediction and detection of Alzheimer's disease dementia. *Eur J Nucl Med Mol Imaging*. 2013;40:1394-1405.
26. Gray KR, Wolz R, Heckemann RA, Aljabar P, Hammers A, Rueckert D. Multi-region analysis of longitudinal FDG-PET for the classification of Alzheimer's disease. *Neuroimage*. 2012;60:221-229.
27. Illan I, Gorriz J, Ramirez J, et al. 18F-FDG PET imaging analysis for computer aided Alzheimer's diagnosis. *Information Sciences*. 2011;181:903-916.
28. Salas-Gonzalez D, Gorriz JM, Ramirez J, et al. Feature selection using factor analysis for Alzheimer's diagnosis using 18F-FDG PET images. *Med Phys*. 2010;37:6084-6095.
29. Pagani M, De Carli F, Morbelli S, et al. Volume of interest-based [18F]fluorodeoxyglucose PET discriminates MCI converting to Alzheimer's disease from healthy controls. A European Alzheimer's Disease Consortium (EADC) study. *Neuroimage Clin*. 2014;18:34-42.
30. Pereira JB, Mijalkov M, Kakaei E, et al. Disrupted Network Topology in Patients with Stable and Progressive Mild Cognitive Impairment and Alzheimer's Disease. *Cereb Cortex*. 2016;26:3476-3493.

31. Laforce R, Jr., Tosun D, Ghosh P, et al. Parallel ICA of FDG-PET and PiB-PET in three conditions with underlying Alzheimer's pathology. *Neuroimage Clin.* 2014;4:508-516.

32. Martinez-Murcia FJ, Gorriz JM, Ramirez J, Puntonet CG, Illan IA. Functional activity maps based on significance measures and Independent Component Analysis. *Comput Methods Programs Biomed.* 2013;111:255-268.

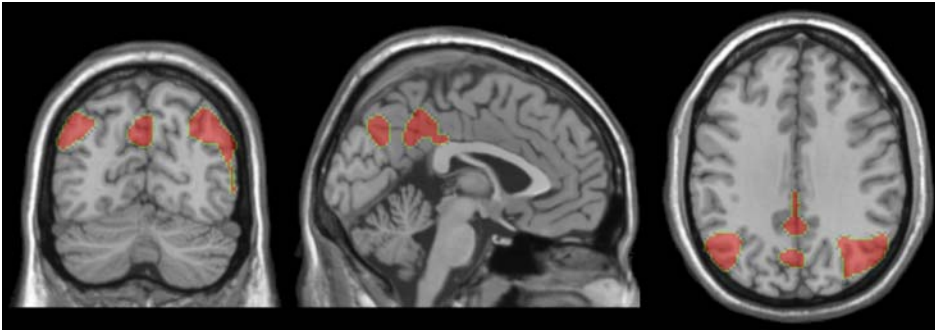


FIGURE 1.

Topographic representation of the Cluster in which FDG uptake was significantly lower in MCI-converting to AD dementia (n=95) than in ncMCI (n=27) (threshold $p < 0.05$, corrected for multiple comparisons with the FWE option). The Cluster is superimposed to the Montreal Neurological Institute template in the coronal (left), sagittal (middle) and transversal (right) views.

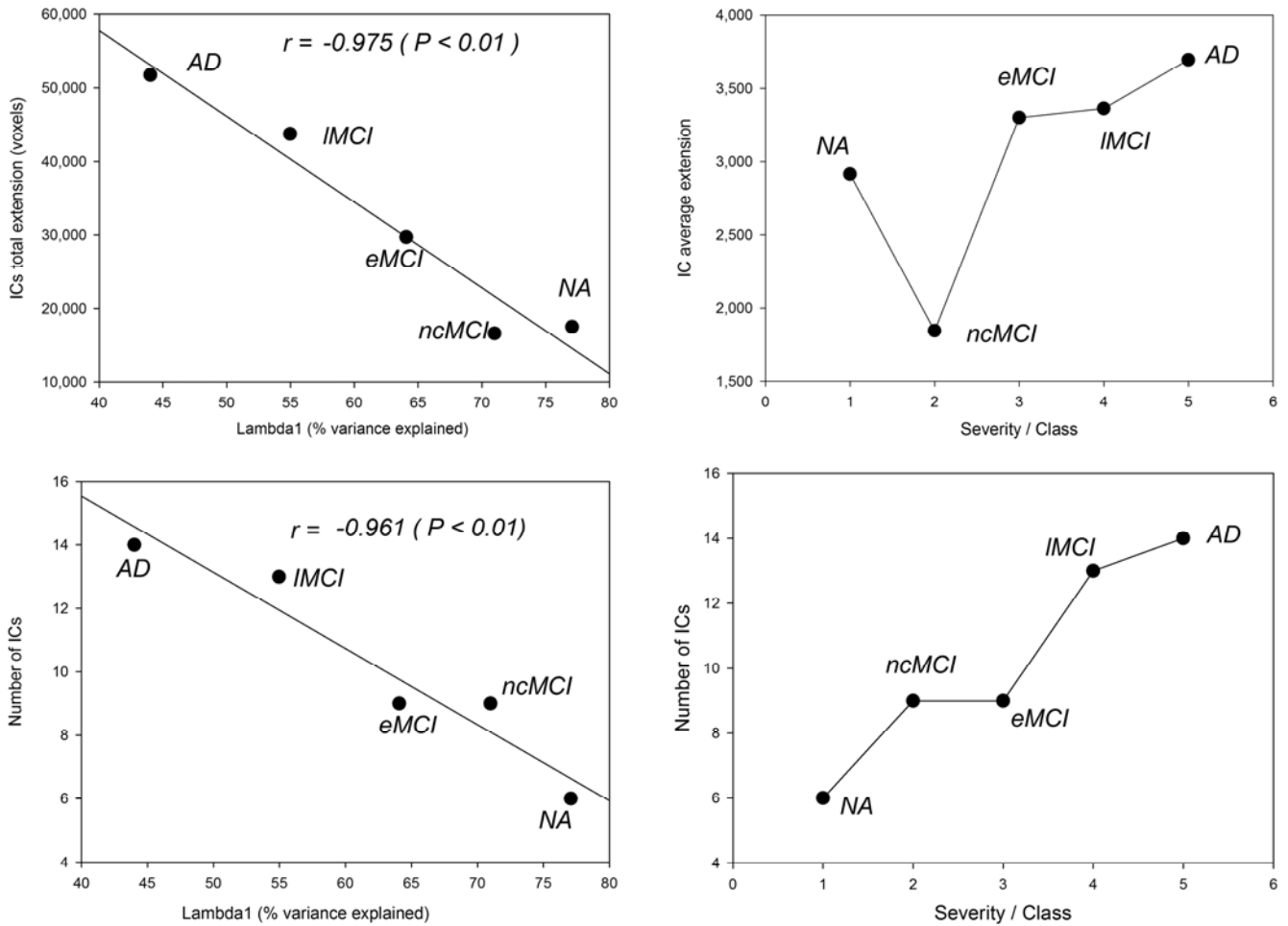


FIGURE 2.

The left side of the figure shows for each severity class the negative correlations between the percent of variance explained by the first principal component (Lambda1) and the generation of local circuits expressed as total ICs extension in voxels (top panel) and number of ICs (bottom panel). The right side shows the relations between the average extension of disease severity class and average IC extension (top panel) and number of ICs (bottom panel).

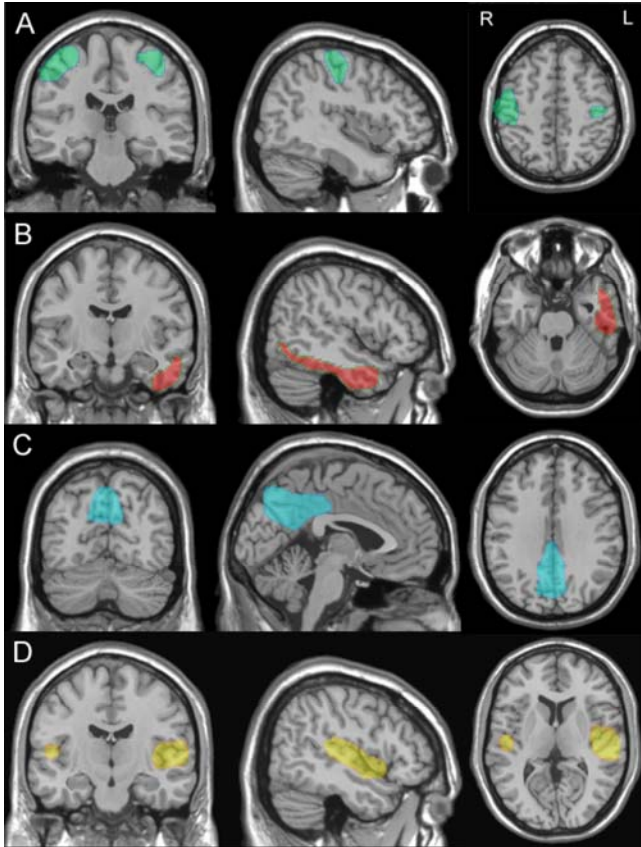


FIGURE 3.

Topographic representations of the ICs identifying the sensorimotor cortex (a), left temporal (b), posterior cingulate cortex/precuneus (c) and sylvian temporal cortex (d) on brain surfaces. The regions obtained from the ICA have been superimposed to the Montreal Neurological Institute template in the coronal (top left), sagittal (top right) and transversal (bottom) views. R=Right; L=Left.

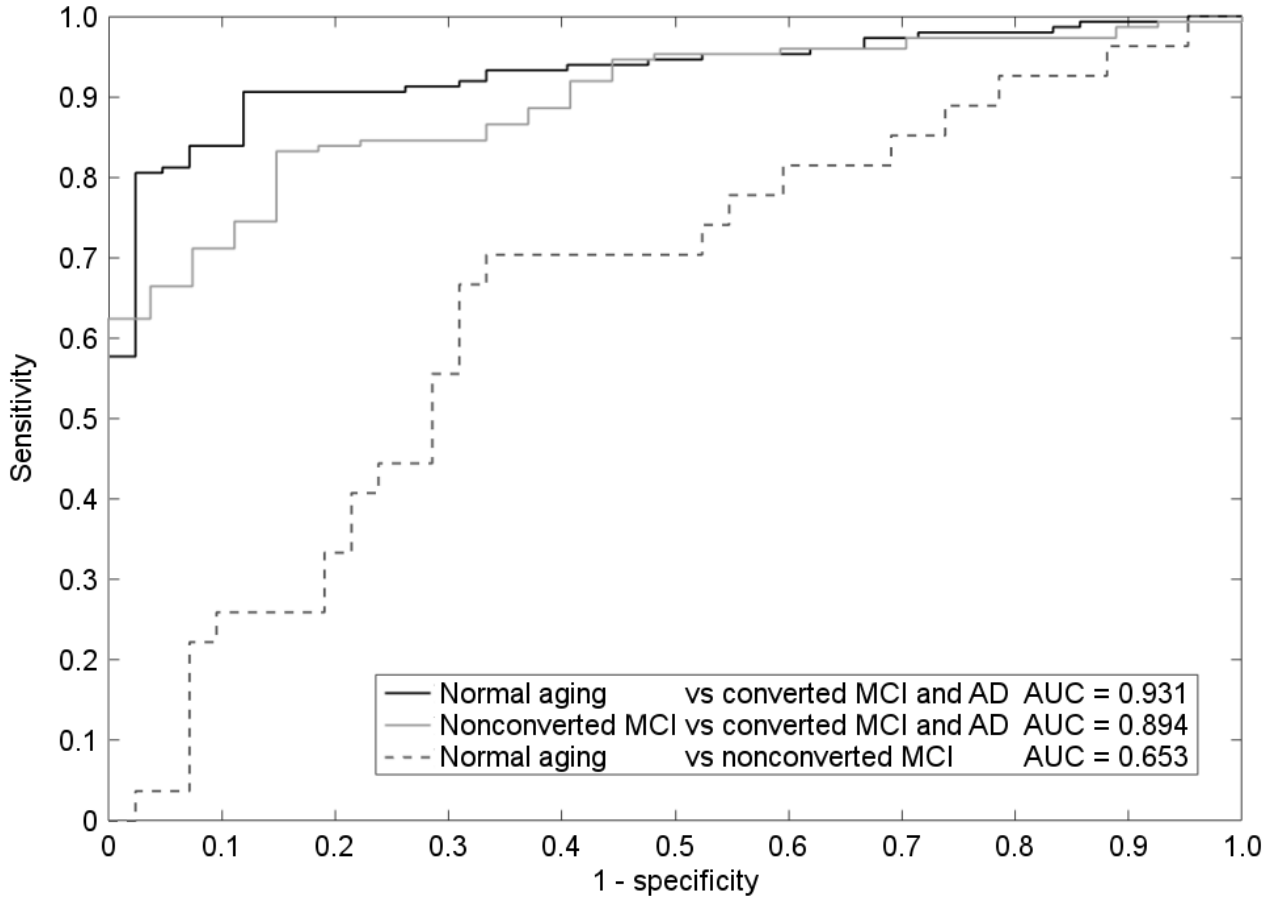


FIGURE 4.

ROC curve obtained by SVM classifier as applied to 3 different datasets: 1) black line: NA versus all patients with Alzheimer pathology (AD), including both MCI converter groups and patients with AD dementia since PET examination; 2) gray line: ncMCI versus all patients with Alzheimer pathology (AD); 3) dotted line: ncMCI versus NA.

TABLE 1. Demographic data

GROUP	EDUCATION (mean±SD)	AGE AT PET (mean±SD)	MMSE (mean±SD)	GENDER (M/F)
NA	10.0±4.1	68.8±9.7	29.1±0.9	12/32
ncMCI	8.9±3.7	71.9±6.4	26.8±1.5	16/12
eMCI	10.4±5.0	74.7±7.0	26.3±1.6	8/28
IMCI	9.9±4.5	75.5±6.5	25.8±1.9	22/36
AD	7.4±4.2	73.4±7.4	19.2±4.0	18/36

Education and Age at PET are expressed in years. Mini Mental Score Examination (MMSE) is normalized for Education. Gender column reports the frequencies of males and females.

TABLE 2. Independent Components identified as pathophysiologically significant in each group

NA		ncMCI		eMCI		IMCI		AD dementia						
SIZE	REGIONS	SIZE	REGIONS	SIZE	REGIONS	SIZE	REGIONS	SIZE	REGIONS					
IC3	2309	DLFC+MFG												
		SMA,												
IC6	907	Premotor and BA9												
IC4	2408	PCC + iPL (DMNpost)	IC 6	3210	PCC + iPL (DMNpost)									
IC14	813	Basal Ganglia					IC 7	1277	Basal Ganglia	IC19	2960	Basal ganglia + Thalami		
IC15	5083	Primary Visual	IC 16	3117	Primary Visual	IC 7	5346	Primary Visual	IC 10	5721	Primary Visual	IC1 e IC9	8783	Primary Visual
IC1	5971	Cerebellum	IC 14	2679	Cerebellum	IC 4	5358	Cerebellum	IC 4	5183	Cerebellum	IC3	5178	Cerebellum
			IC 7	1470	sPL LEFT	IC 1	1756	sPL LEFT + DLFC LEFT + T LEFT						
			IC 8	891	Sensorimotor RIGHT	IC 16	1493	Sensorimotor RIGHT	IC 19	2370	Sensorimotor	IC10	3588	Sensorimotor
			IC 15	1702	Sylvian Temporal	IC 3	4161	Sylvian Temporal	IC 3	4464	Sylvian Temporal	IC8	3121	Sylvian Temporal
			IC 1	1038	DLFC LEFT									
			IC 2	1700	iPL + O									
			IC 12	787	VLFC									
						IC 9	4691	iPL RIGHT + T RIGHT	IC 5	5190	iPL RIGHT + T RIGHT	IC5	4466	iPL + T RIGHT
						IC 17	2922	iPL RIGHT + O RIGHT + T RIGHT				IC15	4000	iPL RIGHT + O RIGHT
						IC 12	1748	Thalami						
						IC 13	2231	O LEFT						
									IC 1	1129	MTL RIGHT	IC6	1357	MTL
									IC 2	2565	VLFC	IC18	3888	VLFC
									IC 6	4427	sPL	IC13	5119	sPL
									IC 12	3700	PCC	IC7	3343	PCC + PC
									IC 8	1894	O			
									IC 9	4281	sPL LEFT + PC + T LEFT			
									IC 13	1526	DLFC			
												IC14	2978	T LEFT
												IC16	2959	T LEFT
SIZE TOT	1749			16594			29706			4372			5174	
	1									7			0	

NA: normal aging; ncMCI: MCI patients not converting to AD at 5 years follow up; eMCI: MCI patients that converted to AD later than 2 years; IMCI: MCI patients that converted to AD within 2 years; AD: patients with mild AD dementia. DLFC = dorsolateral frontal cortex MFG= medial frontal gyrus; SMA= supplementary motor area; PCC = posterior cingulate cortex; BA=Brodmann Area; iPL=inferior parietal lobule; sPL superior parietal lobule; VLFC = ventrolaterale frontal cortex; MTL = mesial temporal lobe; PC = precuneus; O=occipital; T = temporal; DNM=Default Mode Network.

TABLE 3. Discriminant models

Discriminant model	a) NA versus MCI-converters + AD dementia				b) ncMCI versus MCI-converters + AD dementia			
	1 component		4 components		1 component		4 components	
Model performance	Exp.	C.I.	Exp.	C.I.	Exp.	C.I.	Exp.	C.I.
Sensitivity	83.2	77.2-89.2	88.6	83.5-93.7	80.5	74.2-86.9	85.9	80.3-91.5
Specificity	83.3	72.1-94.6	95.2	88.8-100.	74.1	57.5-90.6	77.8	62.1-93.4
Accuracy	83.2	77.9-88.5	90.0	85.8-94.3	79.6	73.6-85.5	84.7	79.3-90.0
ROC-AUC	86.6	79.3-91.8	94.9	90.1-97.3	84.6	76.6-89.9	86.6	78.3-91.9

Within group classification	a)		b)		a)		b)	
	NA	AD	NA	AD	NC	AD	NC	AD
Normal aging (NA)	83.3	16.7	95.2	4.8	85.7	14.3	85.7	14.3
Non converters (NC)	66.7	33.3	81.5	18.5	74.1	25.9	88.9	11.1
Early MCI	27.0	73	16.2	83.8	32.4	67.6	29.7	70.3
Late MCI	17.2	82.8	15.5	84.5	20.7	79.3	25.9	74.1
AD	9.3	90.7	9.3	90.7	11.1	88.9	18.5	81.5

Table 2. Discriminant models as evaluated by leave-one-out cross-validation considering two different partitions into contrasting groups: a) normal aging (NA) versus all patients with Alzheimer disease (AD), both MCI converters and patients with AD dementia since PET examination; b) non-converters-MCI versus all AD patients. Linear discrimination was applied to the best discriminant region (1-component), which in both cases was left temporal cortex. 4-component models were based on Support Vector Machine method and involved in both cases: sensorimotor cortex, left temporal, posterior cingulate cortex/precuneus and sylvian temporal cortex. The two level discrimination as obtained by each model for each group is then reported (within group classification). Gray background color mark groups not involved in the training step. All data are presented in percentage terms. Exp.: expected value. C.I.: confidence interval. ROC-AUC: area under the Receiver-Operating-Characteristic (ROC) curve.